Available online at www.sciencedirect.com
ScienceDirect
Journal of the European Ceramic Society 31 (2011) 763–771
www.elsevier.com/locate/jeurceramsoc

Electrical properties and structure of grain boundaries in n-conducting $BaTiO_3$ ceramics

Junbo Hou [a,b], Zaoli Zhang [b], Wolfgang Preis [a,*], Werner Sitte [a], Gerhard Dehm [b,c]

[a] *Chair of Physical Chemistry, University of Leoben, A-8700 Leoben, Austria*
[b] *Erich Schmid Institute of Materials Science, Austrian Academy of Sciences, A-8700 Leoben, Austria*
[c] *Department of Materials Physics, University of Leoben, A-8700 Leoben, Austria*

Received 16 July 2010; received in revised form 29 October 2010; accepted 21 November 2010
Available online 23 December 2010

Abstract

The electrical properties of positive temperature coefficient (PTC) ceramics are expected to strongly correlate with the potential barrier height at grain boundaries, which in turn may be influenced by the grain boundary structure and chemistry. In this study, n-conducting $BaTiO_3$ ceramics co-doped by La and Mn were prepared, and the electrical properties were determined by impedance spectroscopy and dc four-point van der Pauw measurements. Detailed analysis of the grain boundary structure was performed by electron microscopy techniques across different length scales. The study revealed that the randomly oriented polycrystalline microstructure was dominated by large angle grain boundaries, which in the present case were dry although a secondary crystalline and glass phase formed at triple junctions. The relationship between the observed grain boundary atomic structures and electrical properties is briefly discussed.

Keywords: $BaTiO_3$ and titanates; Electrical properties; Grain boundaries; Interfaces; HRTEM

1. Introduction

As one of the most important electroceramic materials, semiconducting $BaTiO_3$ is widely used in electronic devices such as multilayer ceramic capacitors (MLCCs) and positive temperature coefficient resistors (PTCRs). It is well known that the resistivity of PTC ceramics exhibits a steep rise by several orders of magnitude at the Curie point as temperature increases. The potential barrier height of the double Schottky barriers (DSBs) or space charge layers, formed at the grain boundaries, increases during the ferroelectric-paraelectric phase transition, which is widely accepted as the origin of the PTC-effect in $BaTiO_3$.[1–8] Below the Curie point the surface charges at the grain boundary are compensated by the spontaneous polarization, thus leading to a low room temperature resistance.[2] The concentration of point defects at the grain boundaries, which play a crucial role in forming the DSB, is strongly affected by the preparation conditions.[9–16]

To clarify more accurately the PTC mechanism, the resistivity anomaly of single grain boundaries in $BaTiO_3$-based PTC ceramics was investigated.[17–20] The PTC characteristics of single grain boundaries were found to depend on their orientation. In addition, experimental evidence on bi-crystals indicated that the high-coherent grain boundaries, e.g., low angle and coincidence site lattice boundaries ($\Sigma 3$, $\Sigma 5$, and $\Sigma 9$ grain boundaries) showed low or even no PTC-effect, while the incoherent or random large angle grain boundaries were electrically active.[20–22] Therefore, a sound knowledge of the atomic structure of grain boundaries in PTC ceramics would assist in understanding their electrical properties more precisely.

In this study, La and Mn co-doped $BaTiO_3$ ceramics were prepared and the atomic structure of the various grain boundaries, i.e. random large angle grain boundaries, small angle grain boundaries, and coincident twin boundaries, was carefully characterized by using C_S-corrected high resolution transmission electron microscopy (HRTEM). Additionally, the electrical properties of the bulk and grain boundaries of n-conducting $BaTiO_3$ samples were determined by impedance spectroscopy over a wide temperature range and interpreted in terms of the defect chemistry.

* Corresponding author. Tel.: +43 3842 402 4805; fax: +43 3842 402 4802.
E-mail address: wolfgang.preis@unileoben.ac.at (W. Preis).

0955-2219/$ – see front matter © 2010 Elsevier Ltd. All rights reserved.
doi:10.1016/j.jeurceramsoc.2010.11.016

2. Experimental procedure

Commercial Ti (IV)-isopropoxide (Fluka), $BaCO_3$ (≥99.0%, Fluka), La_2O_3 (≥99.9%, Fluka), and $MnCO_3$ (≥99.99%, Aldrich) were used as starting materials for the sample preparation. Ti (IV)-isopropoxide was hydrolyzed using deionized water (Barnstead, Easypure LF) and then $BaCO_3$, 0.125 mol% La_2O_3 as donor dopant, and 0.05 mol% $MnCO_3$ as acceptor dopant were added. 1.0 mol% TiO_2 was added in excess with respect to the ratio of [Ti]/[Ba] in order to form a liquid phase during sintering. The hydrolyzed dispersion was thoroughly mixed. After evaporation of water the mixture was milled with zirconia balls in a planetary mill (Pulverisette 7, Fritsch GmbH) for 1 h. After drying, the mixture was calcined at 1100 °C for 12 h to form the doped $BaTiO_3$ powder. The composition of the powder was checked by ICP-MS and the actual ratio of La to Mn is 29 to 4. The powder mixed with 2 wt% micronized polyethylene wax (Lanco^{TM} PE1500F, Lubrizol GmbH) was uniaxially pressed into pellets with a pressure of 250 MPa. The green pellet was placed on a platinum foil in an alumina boat and sintered at 1350 °C for 2 h in air. The dimensions of the sintered disc-shaped samples were 1.55 mm thick and 8.5 mm in diameter.

The electrical properties were determined over a wide temperature range ($50 \leq T/°C \leq 800$). Ohmic electrodes for the electrochemical impedance measurements between 50 °C and 600 °C were fabricated by sequentially sputtering 30 nm Cr, 40 nm Ni, and 100 nm Au layers (Cr/Ni/Au). Furthermore, electrodes suitable for the temperature range between 500 °C and 800 °C were fabricated from gold paste (METALOR®, Engelhardt). The sample was loaded between two platinum plates by light spring action. The sample holder was placed in a tube furnace. The sample temperature was measured by K-type thermocouples and the furnace temperature was maintained constant by a temperature controller (Eurotherm 2416). The impedance measurements were conducted over the frequency range from 10 MHz to 10 mHz by using an impedance analyzer (Alpha-A, Novocontrol) with an effective ac voltage of 1.0 V.

In addition, four-point dc measurements were performed between 600 and 850 °C by employing the van der Pauw method. Four peripheral point contacts were applied to a disc-shaped sample (diameter: 8.5 mm, thickness: 0.995 mm) by using platinum paste. The dc measurements were carried out by means of a precision source meter (Keithley 2400) operated in four-wire mode. The sample holder for the van der Pauw measurements was positioned in a horizontal tube furnace, where the temperature close to the sample was measured by type-S thermocouples and the furnace temperature was precisely adjusted by a temperature controller (Eurotherm 2404).

The sample morphology was observed using scanning electron microscopy (SEM; Stereoscan 360, Cambridge Instruments) at an acceleration voltage of 20 kV. The chemical composition was determined by energy dispersive X-ray spectroscopy (EDS; Oxford) in the SEM.

Electron backscatter diffraction (EBSD) was used to investigate the $BaTiO_3$ grain orientation in the polycrystalline samples. This was performed on the mechanically and chemically polished surface using a LEO 1525 field-emission SEM equipped with an EBSD system. The EBSD scan was performed with a step size of 1 μm.

Electron transparent specimens for the transmission electron microscopy (TEM) studies were prepared by polishing and ion milling. The ceramic samples were mechanically polished to a thickness of about 100 μm and then ultrasonically cut into small disks of 3 mm diameter. The disks were dimpled to a thickness of <20 μm and further ion milled to electron transparency at 6 kV. A 200 kV field emission TEM/STEM JEOL 2100F equipped with an image-side C_S-corrector (CEOS) and with an energy filter (Tridiem, Gatan) was used for atomic resolution imaging and high spatial resolution electron energy loss spectroscopy (EELS) analysis. The atomic resolution of this microscope at 200 kV is better than 1.2 Å. The alignment of the C_S-corrector was performed using the CEOS software based on the aberration measurements deduced from Zemlin tableaus. Sufficient small aberration coefficients were achieved before HRTEM images were recorded on a 2 k × 4 k pixel CCD camera. The HRTEM images presented here were obtained from this microscope at an accelerating voltage of 200 kV or 80 kV. Some low magni-

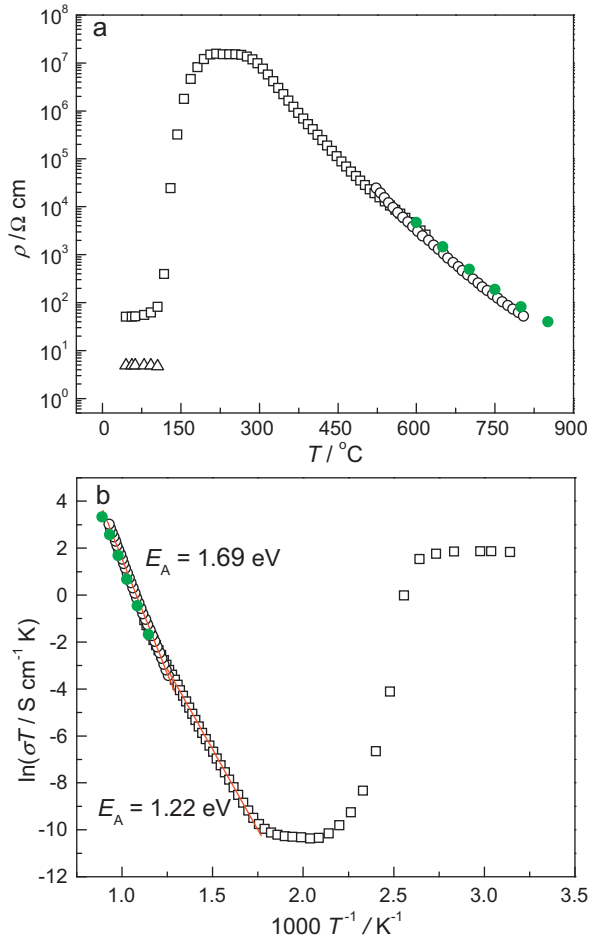

Fig. 1. (a) Bulk and grain boundary resistivities as a function of temperature: (□) grain boundary and (△) bulk resistivities using NiCr/Au electrodes (impedance spectroscopy); (◯) grain boundary resistivities using Au electrodes (impedance spectroscopy); (●) dc four-point van der Pauw measurements. (b) Arrhenius-plot of grain boundary conductivity: solid lines are linear fits.

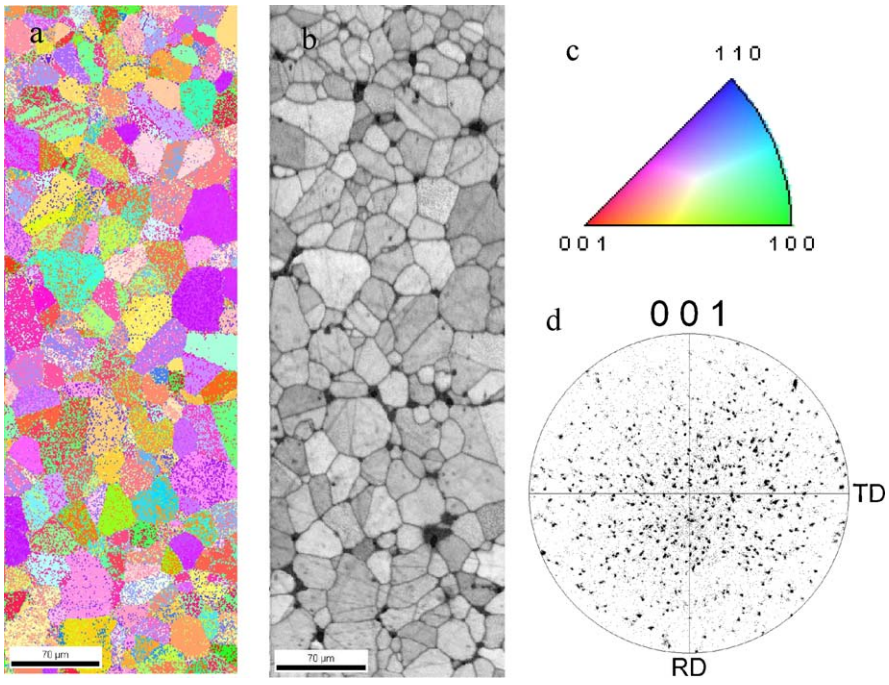

Fig. 2. EBSD pattern: (a) inverse pole figure map (IPFM); (b) image quality map deduced from the quality of the EBSD patterns revealing the grain size; (c) colour key for the crystallographic orientations in the IPFM; (d) contour pole figure (CPF).

fication bright field images were obtained with a Philips CM 12 microscope, operating at an accelerating voltage of 120 kV. Energy-dispersive X-ray spectroscopy (EDS) was used for local chemical composition determination.

3. Results and discussion

3.1. PTC behaviour

The temperature dependence of grain boundary and grain resistances of disc-shaped samples was investigated by electrochemical impedance spectroscopy. The temperature range has been extended to 800 °C by using different electrodes, as shown in Fig. 1. From room temperature to the phase transition temperature (Curie point), the grain boundary resistivity is relatively low with values around 50 Ω cm. The bulk resistance in this region can be accurately de-convoluted by fitting an appropriate equivalent circuit to the impedance data. Typical values of the bulk resistivity are around 4.8 Ω cm. Above the phase transition temperature a rapid growth of the grain boundary resistivity is observed. The highest value is 15.3 MΩ cm. Above approximately 200 °C the negative temperature coefficient (NTC) region is found. The Curie point (T_c) occurs at 105 °C, which is lower than for undoped $BaTiO_3$.

The Arrhenius-plot for the grain boundary conductivity, depicted in Fig. 1b, allows the determination of activation energies for the NTC region ($T > 200$ °C). It should be mentioned that the results of the dc four-point van der Pauw measurements concur well with those obtained from impedance spectroscopy using Au electrodes, which provides further evidence for the reliability of the impedance measurements in the temperature range $500 \leq T/°C \leq 800$. Interestingly, the activa-

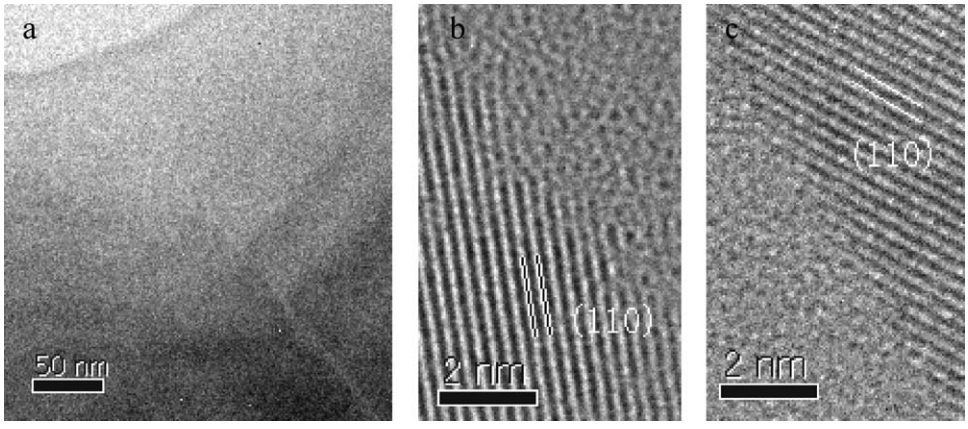

Fig. 3. Typical images of a random large angle grain boundary obtained under 80 keV: (a) bright field image; (b) left grain on zone axis; (c) right grain on zone axis.

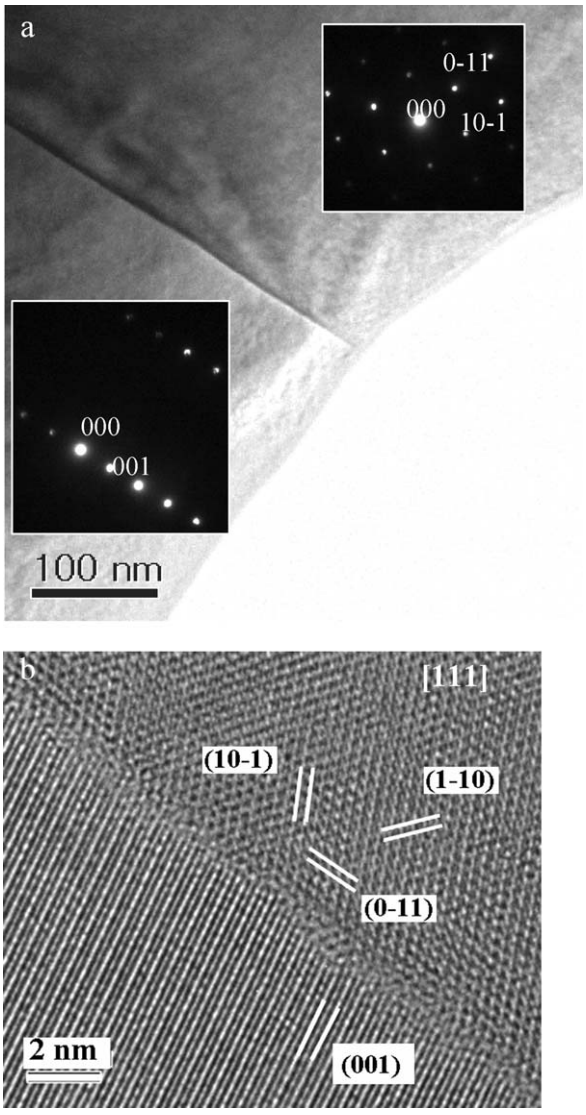

Fig. 4. Random grain boundary image showing both adjacent grains with lattice fringes: (a) bright field image; the insets are the diffraction patterns of the corresponding grains; (b) high resolution image.

tion energy increases from (1.22 ± 0.01) eV to (1.69 ± 0.01) eV at temperatures around 600 °C, as can be seen in Fig. 1b. This behaviour could be interpreted previously by means of an extended Schottky-barrier model.[23] Between 250 and 600 °C the activation energy corresponds to the Schottky-barrier height. In accordance with the Heywang model the PTC effect is accompanied by a rapid increase of the Schottky-barrier height at

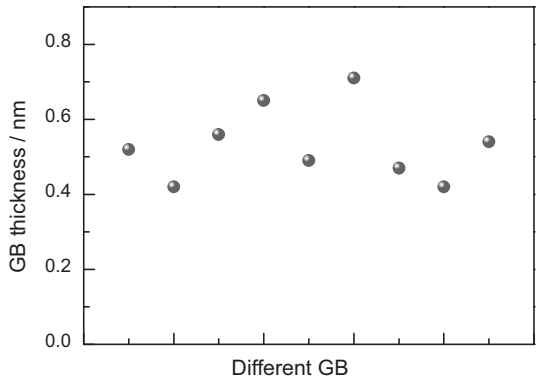

Fig. 6. Apparent grain boundary (GB) thickness estimated from totally 9 random large angle grain boundaries with lattice fringes simultaneously resolved on both adjacent grains.

temperatures higher than the Curie-point. Above approximately 200 °C the barrier height is almost constant leading to the NTC behaviour. The activation energy valid from 600 to 800 °C is close to $E_g/2$ ($E_g = 3.2$ eV[24] refers to the band gap energy). Besides depletion of electrons in the space charge layers the enrichment of holes is anticipated at elevated temperatures. If the concentration of holes exceeds that for electrons in the vicinity of the grain boundary core, the grain boundary resistance is predominantly given by the resistivity of the region with almost equal concentrations of holes and electrons in the space charge layer for comparable hole and electron mobilities,[14] which corresponds to the activation energy of $E_g/2$. More details can be found elsewhere.[23]

3.2. General microstructure

SEM/EBSD was applied to measure the grain orientations of the La and Mn co-doped $BaTiO_3$ (see Fig. 2). The SEM/EBSD map of an area of 544 μm × 190 μm reveals that the sample is polycrystalline with an average grain size of (25 ± 2) μm. No preferred orientation (texture) is observed with the grains revealing a random orientation (Fig. 2a and d). Furthermore, most grains are separated by high angle grain boundaries as revealed by the misorientation between neighbouring grains visualized by the colour code (Fig. 2a and c). The analyzed area contains in total 97 grain boundaries, 86 of them are large angle grain boundaries with misorientations larger than 30° (89%), 2 are small angle grain boundaries (2%), and 9 are twin boundaries (9%).

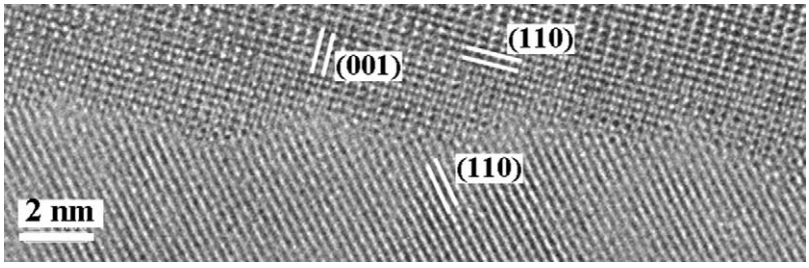

Fig. 5. HRTEM image of a faceted grain boundary.

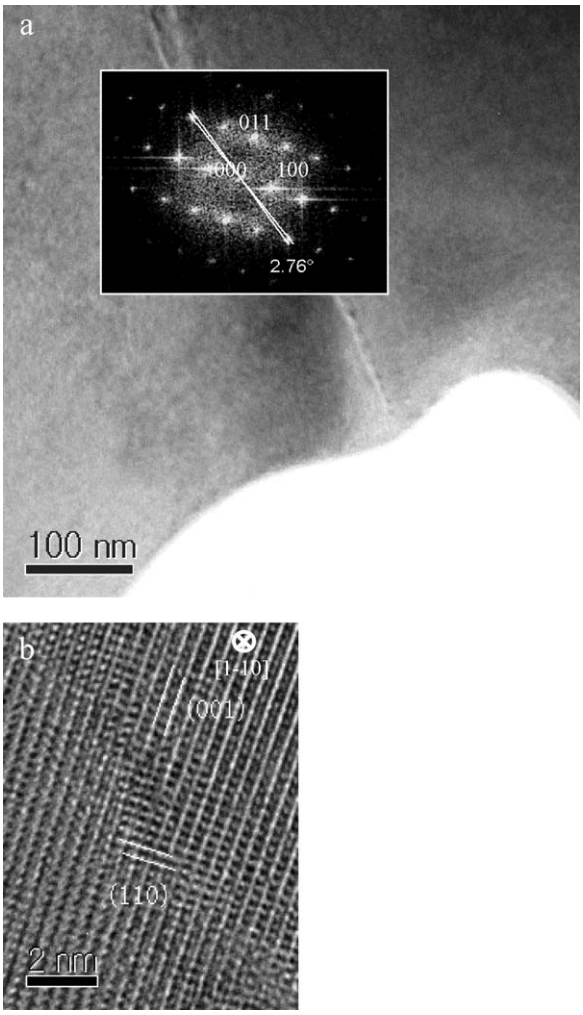

Fig. 7. Small angle grain boundary: (a) bright field image and the diffraction patterns; (b) high resolution image from <1 1 0> direction.

Similar findings were obtained in literature[19,25] with the observation of Kuwabara et al.[19] that a PTC effect in ceramic bars requires a large fraction of random large angle grain boundaries.

All types of grain boundaries were also observed during the HRTEM experiments, where a total of 29 grain boundaries were studied as described below.

3.3. Structure of grain boundaries

In this section we report our observations on 19 random large angle grain boundaries, 8 twin boundaries, and 2 small angle grain boundaries studied by HRTEM. For the large angle grain boundaries HRTEM images often resolved only the lattice structure of one of the adjacent grains (Fig. 3) while a simultaneous observation of the atomic structures of both grains was prevented by their large misorientation. However, in several cases we managed to find random large angle grain boundaries where the lattice fringes were clearly resolved in both grains because each grain is close to a zone axis (see Figs. 4 and 5). It is observed that the grain boundaries can be facetted but always appear dry

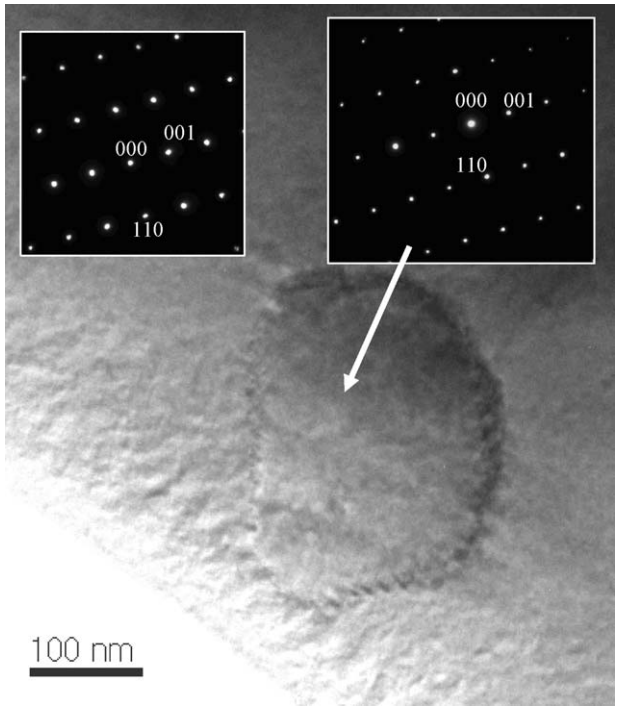

Fig. 8. Subgrain located in the matrix grain with small misorientation: bright field image; insets are matrix diffraction pattern and subgrain diffraction pattern.

devoid of an amorphous glass phase although glass pockets are observed at triple junctions (see Section 3.4).

It has been reported that at 1250 °C most grain boundaries in TiO_2-excess $BaTiO_3$ were faceted.[26] With increasing temperature a transition between faceting and de-faceting will occur.[27] This agrees with our finding that some grain boundaries possess facets for the n-conducting $BaTiO_3$ ceramics sintered at

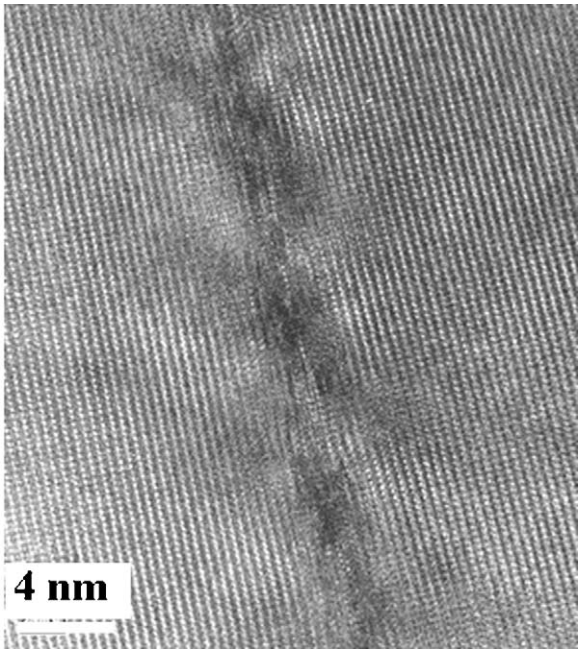

Fig. 9. HRTEM image from the small angle grain boundary between subgrain and matrix grain.

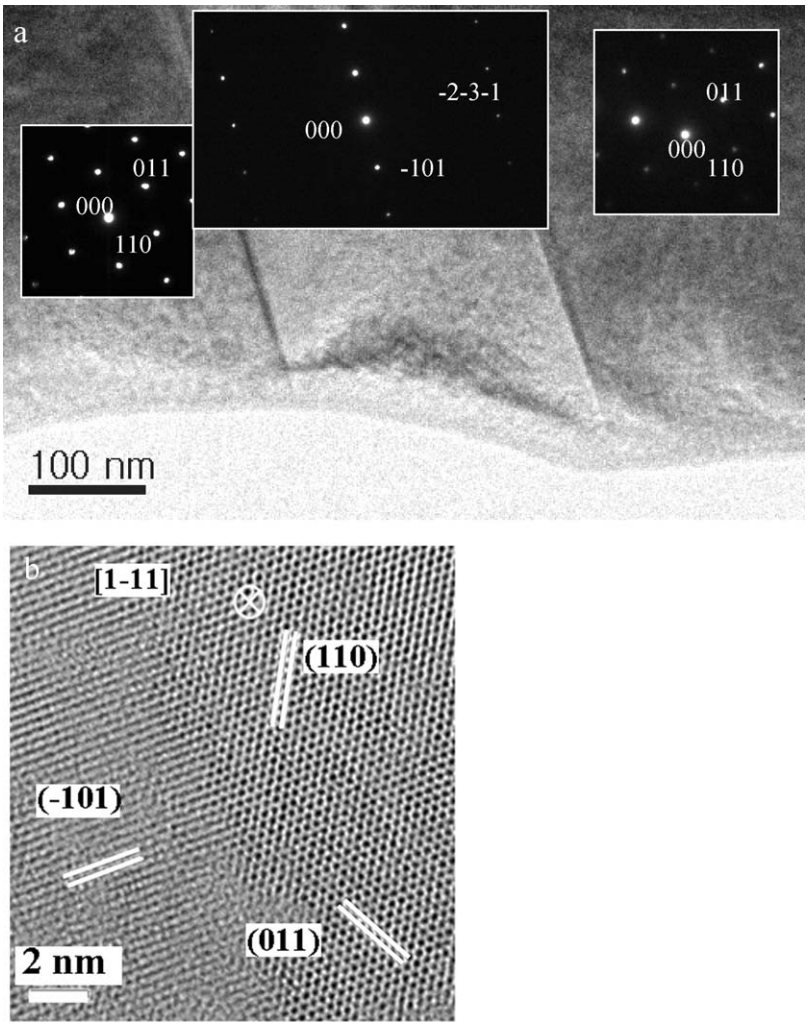

Fig. 10. Twin imaged along <1 1 1> direction: (a) bright field image and diffraction patterns; (b) high resolution image of right twin boundary.

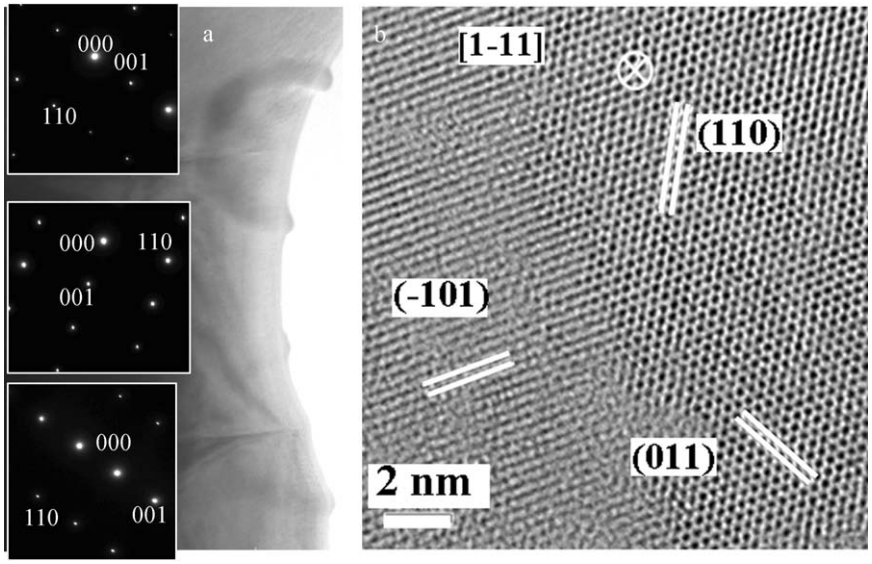

Fig. 11. Twin imaged end-on along <1 1 0> direction: (a) bright field image and diffraction patterns; (b) high resolution image of the lower boundary.

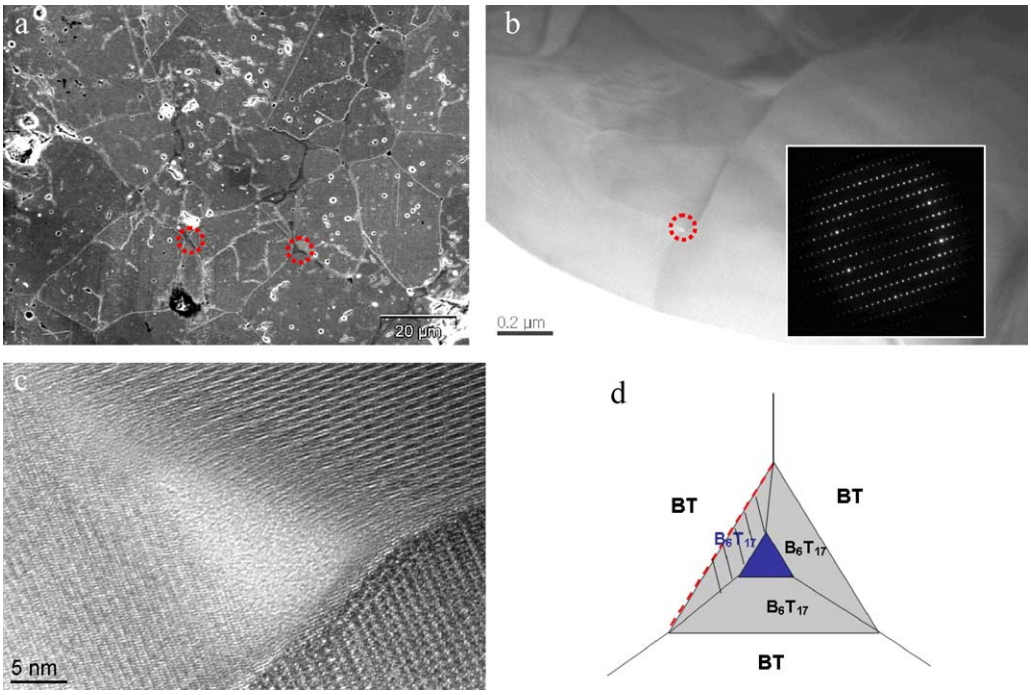

Fig. 12. Micrographs of secondary phase in $BaTiO_3$: (a) SEM image after polishing; (b) bright field TEM image; (c) triple junction of secondary phase; (d) schematic view of triple junction.

1350 °C. In Fig. 5 the grain boundary facets are parallel to the (1 1 0) plane of the upper grain separated by steps following the trace of high indexed planes.

According to the space charge model, the acceptor states at the grain boundary contribute to the potential barrier and hence the PTC effect. A secondary phase layer[17] or an intergranular film[28] was not detected in the present study even when applying Fourier-filter analysis.[29]

From the C_S-corrected HRTEM images such as presented in Fig. 4 where both grains are in or close to a zone axis a direct measure of the apparent width of the grain boundaries was performed. The apparent grain boundary width is taken as the atomically resolved region revealing a thin atomic disordered structural region compared to the neighbouring grains. 9 random large angle grain boundaries could be measured providing an average value of (0.53 ± 0.09) nm with individual values ranging between 0.42 nm and 0.71 nm (Fig. 6). This indicates that the grain boundary thickness is roughly within 1–2 times of the lattice constant. The disordered grain boundary region may contain the acceptor point defects and contribute to the fast oxygen diffusion.[30]

The small angle grain boundaries[31] analyzed in this study reveal dislocations adopting the misorientation between the adjacent grains (Fig. 7). No secondary phases were observed at the small angle grain boundaries and the grain boundary dislocations. In a few cases subgrains were observed (Fig. 8). In general, the size of such subgrain ranges between 100 nm and 1 μm with small misorientations as shown by selected area diffraction studies (see Fig. 8a–c). Fig. 9 shows a HRTEM image taken from a small angle grain boundary between a subgrain and the matrix grain. The dislocation core region is evident and shows very strong lattice distortion (Fig. 9). The subgrain formation and growth by so-called "recrystallization"[32] is noticed only rarely for $BaTiO_3$ ceramics. With respect to the electrical properties, however, such subgrains with small angle grain boundaries might show a negligible PTC-effect and therefore should be avoided.

Twins are commonly found in $BaTiO_3$ ceramics,[33–36] and are also observed in this study (Figs. 10 and 11). The detected twin lamella (Fig. 10) is about 200 nm wide and embedded in a 20 μm large matrix grain. The twin boundary plane is {1 1 1} as shown in the HRTEM image recorded edge-on along [1–10] zone axis (Fig. 11). Twins are usually formed during the solid state reaction of $BaCO_3$ and TiO_2, and are expected to appear especially in abnormally grown grains.[35,37,38]

3.4. Secondary phase

Above the eutectic temperature of $BaTiO_3$ and $Ba_6Ti_{17}O_{40}$ (1332 °C), TiO_2-excess $BaTiO_3$ can intrinsically form the Ti-rich phase. Also during the cooling process, the re-oxidation of the reduced and semiconducting state of the donor doped $BaTiO_3$ would readily transform from electron compensation to cation compensation at the grain boundary region:

$$Ti_{Ti} + O_2 + 4e' \leftrightarrow TiO_2 + V'''_{Ti} \quad (1)$$

The crystalline secondary phase can be found in the sample, as shown in Fig. 12. The Ti-excess was confirmed by EDS. From SEM and low magnification TEM images (Fig. 12a and b), it is

clear that the secondary phase is located at the triple junctions of $BaTiO_3$. TEM proofs by SAED and lattice imaging that the secondary phase is crystalline (Fig. 12b and c). Interestingly, an amorphous phase is located at the centre of the triple junction of $BaTiO_3$ adjacent to the crystalline secondary phase $Ba_6Ti_{17}O_{40}$ (Fig. 12c). The morphology is schematically shown in Fig. 12d.

The secondary phase precipitation in the matrix grains was previously reported.[39,40] In this study, however, the secondary phase is only found to be located at the triple junction.

Although no intergranular films of secondary phase are observed, the random large angle grain boundaries seem to consist of a disordered layer with an apparent width of 1–2 lattice constants. Segregation of Mn at these grain boundaries may give rise to the interfacial acceptor states necessary for the PTC-effect. However, the Mn-concentration (0.05 at%) in this study is quite low which we could not detect using EELS. Mn-segregation will be studied systematically in the future on samples containing a higher amount of dopants. In addition, it should be mentioned that recently the PTC-effect has been reported to occur only at large angle grain boundaries.[21] This finding agrees well with our observations, where a strong PTC effect was measured in n-conducting $BaTiO_3$ ceramics containing mainly large angle grain boundaries.

4. Conclusions

The microstructure and grain boundary structure of n-conducting $BaTiO_3$ ceramics, which was prepared by a modified solid state reaction method, were characterized by electron microscopy techniques including grain misorientation analysis by EBSD/SEM and atomic resolved imaging using C_S-corrected HRTEM. A secondary crystalline $Ba_6Ti_{17}O_{40}$ phase and an amorphous glass phase were observed at the triple junctions between $BaTiO_3$ grains. A systematic study of 29 grain boundaries by HRTEM revealed no remarkable amorphous intergranular film. The majority of grain boundaries in the polycrystalline ceramics were with 89% large angle grain boundaries, which possess on average an apparent width of ~0.53 nm. Impedance measurements reveal a change in the activation energy from (1.22 ± 0.01) eV to (1.69 ± 0.01) eV at approximately 600 °C implying that the grain boundary resistance is influenced by the enriched holes in the space charge layer at elevated temperatures.

Acknowledgements

Financial support by the Austrian Federal Government and the Styrian Provincial Government, represented by Österreichische Forschungsförderungsgesellschaft mbH and Steirische Wirtschaftsförderungsgesellschaft mbH, within the research activities of the K2 Competence Centre on "Integrated Research in Materials, Processing and Product Engineering", operated by the Materials Center Leoben Forschung GmbH under the frame of the Austrian COMET Competence Centre Programme, is gratefully acknowledged. The authors are grateful to Dr. Jerzy Bugajski for his help in materials synthesis and Dr. Martin Rester for the EBSD measurements.

References

1. Heywang W. Resistivity anomaly in doped barium titanate. *J Am Ceram Soc* 1964;**47**:484–90.
2. Jonker GH. Some aspects of semiconducting barium titanate. *Solid-State Electron* 1964;**7**:895–903.
3. Daniels J, Wernicke R. Part V. New aspects of an improved PTC model. *Philips Res Reports* 1976;**31**:544–59.
4. Ihrig H, Puschert W. A Systematic experimental and theoretical investigation of the grain-boundary resistivities of n-doped $BaTiO_3$ ceramics. *J Appl Phys* 1977;**48**:3081–8.
5. Lewis GV, Catlow CRA, Casselton REW. PTCR effect in $BaTiO_3$. *J Am Ceram Soc* 1985;**68**:555–8.
6. Alles AB, Burdick VL. Grain boundary oxidation in PTCR barium titanate thermistors. *J Am Ceram Soc* 1993;**76**:401–8.
7. Smyth DM. The defect chemistry of donor-doped $BaTiO_3$: a rebuttal. *J Electroceram* 2002;**9**:179–86.
8. Preis W, Bürgermeister A, Sitte W, Supancic P. Bulk and grain boundary resistivities of donor-doped barium titanate ceramics. *Solid State Ionics* 2004;**173**:69–75.
9. Kulwicki BM, Purdes AJ. Diffusion potentials in $BaTiO_3$ and the theory of PTC materials. *Ferroelectrics* 1970;**1**:253–63.
10. Daniels J, Härdtl KH. Part I. Electrical conductivity at high temperatures of donor-doped barium titanate ceramics. *Philips Res Reports* 1976;**31**:489–504.
11. Wernicke R. Part IV. The kinetics of equilibrium restoration in barium titanate ceramics. *Philips Res Reports* 1976;**31**:526–43.
12. Ting CJ, Peng CJ, Lu HY, Wu ST. Lanthanum–magnesium and lanthanum–manganese donor–acceptor-codoped semiconducting barium titanate. *J Am Ceram Soc* 1990;**73**:329–34.
13. Chiang YM, Takagi T. Grain-boundary chemistry of barium titanate and strontium titanate. II. Origin of electrical barriers in positive-temperature-coefficient thermistors. *J Am Ceram Soc* 1990;**73**:3286–91.
14. Waser R, Hagenbeck R. Grain boundaries in dielectric and mixed-conducting ceramics. *Acta Mater* 2000;**48**:797–825.
15. Gallego MM, West AR. Effect of annealing treatments on positive temperature coefficient of resistance properties of barium titanate ceramics and a new model for the positive temperature coefficient of resistance effect. *J Appl Phys* 2001;**90**:394–403.
16. Preis W, Sitte W. Modelling of grain boundary resistivities of n-conducting $BaTiO_3$ ceramics. *Solid State Ionics* 2006;**177**:2549–53.
17. Gerthsen P, Hoffmann B. Current–voltage characteristics and capacitance of single grain boundaries in semiconducting $BaTiO_3$ ceramics. *Solid State Electron* 1973;**16**:617–22.
18. Nemoto H, Oda I. Direct examination of PTC action of single grain boundaries in semiconducting $BaTiO_3$ ceramics. *J Am Ceram Soc* 1980;**63**:398–401.
19. Kuwabara M, Morimo K, Matsunaga T. Single-grain boundaries in PTC resistors. *J Am Ceram Soc* 1996;**79**:997–1001.
20. Hayashi K, Yamamoto T, Sakuma T. Grain orientation dependence of the PTCR effect in niobium-doped barium titanate. *J Am Ceram Soc* 1996;**79**:1669–72.
21. Hayashi K, Yamamoto T, Ikuhara Y, Sakuma T. Formation of potential barrier related to grain-boundary character in semiconducting barium titanate. *J Am Ceram Soc* 2000;**83**:2684–8.
22. Choi SY, Buban J, Nishi M, Kageyama H, Shibata N, Yamamoto T, et al. Dislocation structure of low-angle boundaries in Nb-doped $SrTiO_3$ bicrystals. *J Mater Sci* 2006;**41**:2621–5.
23. Preis W, Sitte W. Modeling of transport properties of interfacially controlled electroceramics: application to n-conducting barium titanate. *J Electroceram* 2010, doi:10.1007/s10832-009-9577-8.
24. Yoo HI, Song CR, Lee DK. $BaTiO_{3-\delta}$: defect structure, electrical conductivity, chemical diffusivity, thermoelectric power, and oxygen nonstoichiometry. *J Electroceram* 2002;**8**:5–36.

25. Ernst F, Mulvihill M, Kienzle O, Rühle M. Preferred grain orientation relationships in sintered perovskite ceramics. *J Am Ceram Soc* 2001;**84**:1885–90.
26. Lee BK, Chung SY, Kang SJL. Grain boundary faceting and abnormal grain growth in $BaTiO_3$. *Acta Mater* 2000;**48**:1575–80.
27. Lee SB, Choi SY, Kang SJL, Yoon DY. TEM observations of singular grain boundaries and their roughening transition in TiO_2-excess $BaTiO_3$. *Z Metallkd* 2003;**94**:193–9.
28. Choi SY, Yoon DY, Kang SJL. Kinetic formation and thickening of intergranular amorphous films at grain boundaries in barium titanate. *Acta Mater* 2004;**52**:3721–6.
29. Zhang Z, Sigle W, De Souza RA, Kurtz W, Maier J, Rühle M. Comparative studies of microstructure and impedance of small-angle symmetrical and asymmetrical grain boundaries in $SrTiO_3$. *Acta Mater* 2005;**53**: 5007–15.
30. Preis W. Fast grain boundary diffusion and surface exchange reactions at active surface sites of polycrystalline materials. *Phys Chem Chem Phys* 2006;**8**:2629–34.
31. Cho YK, Yoon DY. Faceting of high-angle grain boundaries in titanium-excess $BaTiO_3$. *J Am Ceram Soc* 2004;**87**:438–42.
32. Doherty RD, Hughes DA, Humphreys FJ, Jonas JJ, Jensen DJ, Kassner ME, et al. Current issues in recrystallization: a review. *Mater Sci Eng A* 1997;**238**:219–74.
33. Oppolzer H, Schmelz H. Investigation of twin lamellae in $BaTiO_3$ ceramics. *J Am Ceram Soc* 1983;**66**:444–6.
34. Schmelz H, Thomann H. Twinning in $BaTiO_3$ ceramics. *Ceram Forum Int* 1984;**61**:199–204.
35. Eibl O, Pongratz P, Skalicky P, Schmelz H. Formation of (1 1 1) twins in $BaTiO_3$ ceramics. *J Am Ceram Soc* 1987;**70**:C-195–7.
36. Kästner G, Wagner R, Lacayo G, Hilarius V. Twins and grain growth during liquid-phase sintering of $BaTiO_3$ ceramics. *J Mater Sci Lett* 1989;**8**:802–4.
37. Kresevec V, Drofenik M, Kolar D. Genesis of the (1 1 1) twin in barium titanate. *J Am Ceram Soc* 1990;**73**:856–60.
38. Seaton J, Leach C. Formation and retention of low Σ interfaces in PTC thermistors. *Acta Mater* 2005;**53**:2751–8.
39. Makovec D, Drofenik M. Microstructural changes during the reduction/reoxidation process in donor-doped $BaTiO_3$ ceramics. *J Am Ceram Soc* 2000;**83**:2593–9.
40. Makovec D, Ule N, Drofenik M. Positive temperature coefficient of resistivity effect in highly donor-doped barium titanate. *J Am Ceram Soc* 2001;**84**:1273–80.